

A combined density functional theory and interatomic potential-based simulation study of the hydration of nano-particulate silicate surfaces

Zhimei Du ^a, Nora H. de Leeuw ^{a,b,*}

^a School of Crystallography, Birkbeck College, University of London, Malet Street, London WC1E 7HX, UK

^b Department of Chemistry, University College London, 20 Gordon Street, London WC1H 0AJ, UK

Received 27 November 2003; accepted for publication 4 February 2004

Abstract

Density functional theory (DFT) calculations as well as interatomic potential-based simulations have been employed to study the adsorption of water at two α -quartz (0001) surfaces. The different methods are found to be in agreement, both as to modes and energies of adsorption. When under-coordinated surface silicon and oxygen atoms are present, water adsorbs dissociatively at the surface, thereby annihilating dangling bonds by the formation of surface hydroxy groups. However, when the surface species are linked by Si–O–Si bridges and fully coordinated, water adsorbs associatively, releasing approximately 40 kJ mol⁻¹. The comparison study shows that the use of complementary computational techniques is efficient in identifying and investigating low-energy surface features and behaviour. The potential model for hydrated silica performs sufficiently well to be suitable for use in further simulations of the hydration of a silicate nano-tube. Results of these calculations show that the side of the nano-tube is relatively resistant against dissociative chemisorption and silicon dissolution, but that the end of the nano-tube is highly reactive towards water and amenable to dissolution.

© 2004 Elsevier B.V. All rights reserved.

Keywords: Density functional calculations; Computer simulations; Silicon oxides; Chemisorption; Surface structure, morphology, roughness, and topography; Surface electronic phenomena (work function, surface potential, surface states, etc.)

1. Introduction

With the onset of applications of nano-scale materials in, for example, modern catalytic processes, research into structure/property relationships of promising materials such as carbon and oxide nano-particles has increased dramatically, e.g. Ref. [1]. This field is particularly suitable for investigation by modern computational techniques as experimental studies of many chemical phenomena at this scale are still difficult to perform.

* Corresponding author. Address: School of Crystallography, Birkbeck College, University of London, Malet Street, London WC1E 7HX, UK. Tel.: +44-20-7679-1015; fax: +44-20-7631-6803.

E-mail addresses: z.du@mail.cryst.bbk.ac.uk (Z. Du), n.deleeuw@mail.cryst.bbk.ac.uk, n.h.deleeuw@ucl.ac.uk (N.H. de Leeuw).

SiO₂ is a material with interesting properties on many different length scales and given its importance in electronic, optical and biomedical applications, as well as its dominance in geological environments, it has particular appeal to a variety of scientific communities. In recent years, many unusual silica nano-structures have been synthesized by a variety of methods, from vapour deposition of silica thin films [2], ribbons [3] and wires [4] through the hydrothermal synthesis of quartz nano-crystals [5] to templated sol-gel techniques for the production of smart silica nanotubes for biomedical applications [6].

The presence of water in the lattice affects physical properties such as diffusion rates and melting points, and is well known to reduce the crystal strength of bulk silicate materials (hydrolytic weakening) [7] allowing deformation of the crystal. The interaction of water with the bulk material has been investigated both computationally and experimentally [8–13], while anhydrous silicate surfaces have been studied more recently [14–18]. However, although the interaction of water with silicate clusters [19,20] and vitreous silica interfaces [16,17,21] has been studied computationally, to the authors' knowledge little or no work has been reported on water adsorption at the α -quartz surface using electronic structure calculations, although interatomic potential-based methods have successfully modelled the water interface with α -quartz and β -quartz [15,22] and cristobalite [23]. In this work we present detailed electronic structure calculations of the interaction of water with two α -quartz (0001) surfaces. In addition, we compare these calculations with interatomic potential-based methods, which are then further employed to study the hydration and possible dissolution of a nano-tube structure. We have employed this combined approach of electronic structure calculations based on the density functional theory and interatomic potential-based simulations to firstly investigate the electronic structure and chemical reactivity of a slab of α -quartz material and, secondly, to verify the adequacy of the potential model used in the further study of the hydration and onset of dissolution of the nano-tube, with a view to determining whether the silica tube is a stable structure in the presence

of water vapour and as such whether we could expect it to be synthesized in the future.

2. Theoretical methods

Computational methods are well placed to calculate at the atomic level the geometries and adsorption energies of water at the silicate surfaces. We have employed established density functional theory (DFT) methods, which generally achieve a good balance between accuracy and computational expense, to study the structure and energetics of hydration of a thin slab of α -quartz material. The basic concepts of DFT and the principles of its application to pseudo-potential plane-wave calculations have been extensively reviewed elsewhere [24–26]. This technique is now well established and has been successfully applied to the study of a wide range of materials from metals, e.g. [27,28], to (semi-) ionic solids, e.g. [29–31].

The Vienna *ab initio* simulation program (VASP) [32–35] was used for the DFT calculations, which employs ultra-soft pseudo-potentials for the effective interaction of the valence electrons with the atomic cores [36,37], hence allowing a smaller basis set for a given accuracy. In our calculations the core consisted of orbitals up to and including the 1s orbital for oxygen and the 2p orbital for silicon, while hydrogen has no core. The valence orbitals are represented by a plane-wave basis set, in which the energy of the plane waves is less than a given cutoff (E_{cut}). The degree of convergence of the total energy depends on several factors, such as the plane-wave cutoff and the density of k -point sampling within the Brillouin zone. The magnitude of E_{cut} required to converge the total energy of the system has important implications for the size of the calculation. We carried out a number of investigations for the bulk material to determine the values for E_{cut} (300 eV) and the size of the Monkhorst-Pack k -point mesh ($1 \times 1 \times 1$), so that the total energy is converged to within 0.5 eV (<0.7%). The calculations were performed within the generalized-gradient approximation, using the exchange-correlation potential of Perdew et al. [38]. In the course of our DFT study, we firstly performed the

optimization of the bulk material, where a conjugate gradients algorithm is used for the geometry optimization. The surface was modelled as a slab of material and separated by a vacuum gap from its images using three-dimensional periodic boundary conditions. To test convergence of these simulations, calculations were conducted for a series of slab thicknesses and gap widths and these convergence tests showed that a slab thickness of three unit cells deep, i.e. approximately 16 Å, together with a gap width of about 10 Å were sufficient for the surface calculations to be convergent, which agreed with previous adsorbate/substrate calculations using the VASP code on both metallic and ionic systems (e.g. [39,40]). As a result of these test calculations, we ensured that all simulations were carried out with a gap of at least 10 Å of vacuum between the surface on one side of the slab, together with any adsorbed water, and the next (hydrated) surface across the void. The area of the surface unit cell, i.e. the size of the slab in the *ab* plane, was 24.1 Å² which simulation cell was infinitely repeated in two dimensions parallel to the surface and hence we did not need to check for convergence with size in these directions.

The simulation code METADISE [41] was used in the interatomic potential-based simulations for both adsorption of water on the same slab of quartz and for the simulations of the nano-tube structure. The code is designed to model dislocations, interfaces and surfaces and it is based on the Born model of solids which assumes that the ions in the solid interact via long-range electrostatic forces and short-range forces including both the repulsions and the van der Waals attractions between neighbouring electron charge clouds [42]. The shell model of Dick and Overhauser is used to take into account polarization of relevant ions, in our case the oxygen ion, which is treated as a massive core linked to a massless shell by a harmonic spring [43]. We used the potentials model derived by Sanders et al. [11] for the simulation of the silicate structures with the water potential of Baram and Parker [44] and de Leeuw and Parker [45] for the dissociated and associated water molecules respectively. The interaction parameters between the water molecules and the silicate

structures were taken from the study of hydrated quartz surfaces by de Leeuw et al. [15], but the interactions between the silicon atom and oxygen atom of the water molecule were refined for this work in the light of our comparative DFT calculations. The complete potential model is listed in Table 1. The hydration energy of the SiO₂ slab or nano-tube is given by Eq. (1):

$$E_{\text{hydr}} = E_{\text{SiO}_2+\text{wat}} - (E_{\text{SiO}_2} + E_{\text{H}_2\text{O}}) \quad (1)$$

where E_{hydr} is the energy of adsorption of a water molecule at the surface of the SiO₂ slab or nano-tube (hydration energy), $E_{\text{SiO}_2+\text{wat}}$ and E_{SiO_2} are the calculated energies of the hydrated and dehydrated slab or nano-tube respectively, and $E_{\text{H}_2\text{O}}$ is the self-energy of water. For the DFT calculations, $E_{\text{H}_2\text{O}}$ is simply the energy of the isolated water molecule (−1325.7 kJ mol^{−1}). The energy of the water molecule is determined using an equivalent supercell and the same simulation parameters as in the calculation of the whole system to achieve cancellation of basis set errors. In the interatomic potential-based calculations of associative adsorption of water, $E_{\text{H}_2\text{O}}$ of the adsorbed water molecule is also straightforward and calculated at −869.8 kJ mol^{−1}.

However, calculation of the dissociative adsorption of water using the potential-based methods is less straightforward. Here, the energy of dissociation of the molecule is required as well, but this reaction requires the second electron affinity of oxygen, which is material-dependent. However, this energy can be obtained from an energy cycle using experimental enthalpies for some of the reactions, as shown below:

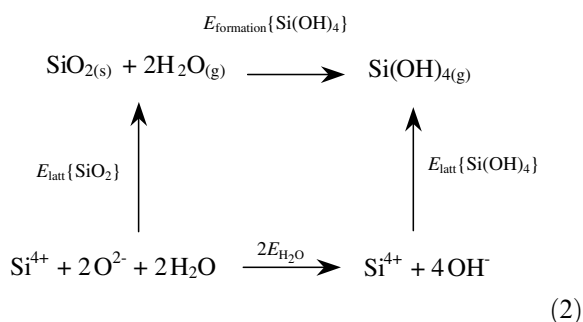
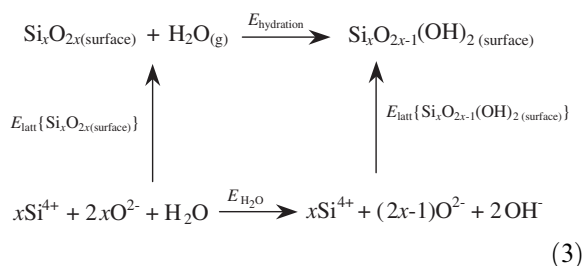


Table 1
Interatomic potential model used in this work (short range cut-off 20 Å)

Charges (e)			Core-shell interaction (eV Å ⁻²)
Ion	Core	Shell	
Si	+4.00000		
H	+0.40000		
Silicate oxygen	+ 0.84819	-2.84819	74.92038
Hydroxy oxygen	+0.90000	-2.300	74.92038
Water oxygen	+1.25000	-2.050	209.4496
<i>Buckingham potential</i>			
Inter-molecular	A (eV)	ρ (Å)	C (eV Å ⁶)
Si ⁴⁺ -O ²⁻	1283.91	0.32052	10.66158
Si ⁴⁺ -O ^{1.4-}	983.56	0.32052	10.66158
Si ⁴⁺ -O ^{0.8-}	983.56	0.32052	10.66158
O ²⁻ -O ²⁻	22764.0	0.14900	27.88
O ²⁻ -O ^{1.4-}	22764.0	0.14900	13.94
O ²⁻ -O ^{0.8-}	22764.0	0.14900	28.92
O ^{1.4-} -O ^{1.4-}	22764.0	0.14900	6.97
O ^{1.4-} -O ^{0.8-}	22764.0	0.14900	17.14
H ^{0.4+} -O ²⁻	396.27	0.25	0.0
H ^{0.4+} -O ^{1.4-}	311.97	0.25	0.0
H ^{0.4+} -O ^{0.8-}	396.27	0.25	10.0
<i>Lennard-Jones potential</i>			
	A (eV Å ¹²)		B (eV Å ⁶)
O ^{0.8-} -O ^{0.8-}	39344.98		42.15
<i>Morse potential</i>			
Intra-molecular	D (eV)	α (Å ⁻¹)	r_0 (Å)
H ^{0.4+} -O ^{1.4-} _{shell}	7.052500	3.17490	0.92580
H ^{0.4+} -O ^{0.8-} _{shell}	6.203713	2.22003	0.92376
<i>Three-body potential</i>			
	K (eV rad ⁻²)		Θ_0
O ²⁻ _{shell} -Si-O ²⁻ _{shell}	2.09724		109.470000
H ^{0.4+} -O ^{0.8-} _{shell} -H ^{0.4+}	4.19978		108.693195
<i>Intra-molecular coulombic interaction (%)</i>			
H ^{0.4+} -O ^{0.8-}	50		
H ^{0.4+} -H ^{0.4+}	50		

where $E_{\text{formation}} \{\text{Si}(\text{OH})_4\}$ is the heat of formation of silicic acid $\text{Si}(\text{OH})_4$ which was found to be 11.7 kJ mol⁻¹ [46], $E_{\text{latt}} \{\text{Si}(\text{OH})_4\}$ and $E_{\text{latt}} \{\text{SiO}_2\}$ are the lattice energies of $\text{Si}(\text{OH})_4$ and SiO_2 , which were calculated to be -10784.6 and -12413.7 kJ mol⁻¹ respectively. We can now use the energy of the reaction of one oxygen with one water molecule to form two hydroxy groups ($E_{\text{H}_2\text{O}} = -808.7$ kJ mol⁻¹), to calculate the energy released (per water molecule) upon adsorption of dissociative water at the silica surface as follows:



where $E_{\text{latt}} \{\text{Si}_x\text{O}_{2x(\text{surface})}\}$ is the energy of the unhydrated surface slab (or nano-tube) obtained

from the simulations, $E_{\text{latt}}\{\text{Si}_x\text{O}_{2x-1}(\text{OH})_{2(\text{surface})}\}$ is the energy of the hydroxylated surface slab (or nano-tube), also obtained from the simulations, and $E_{\text{H}_2\text{O}}$ is the energy of dissociation of one water molecule obtained from cycle (2) above. The hydration energy of dissociative adsorption of water at the surface thus can be obtained for each surface configuration directly from this energy cycle (3).

The surface energy of a surface is a measurement of its thermodynamic stability, where a low and positive value indicates a stable surface. For a dry surface the surface energy is given by

$$\gamma = \frac{U_S - U_B}{A} \quad (4)$$

where U_S is the energy of the surface block of the crystal, U_B is the energy of an equal number of atoms of the bulk crystal and A is the surface area. Experimentally, the surface energy is thus the energy required to cleave the crystal, exposing the surface. For the hydrated surfaces the surface energies were calculated with respect to liquid water in order to assess the stability of the surfaces in an aqueous environment, using the following equation:

$$\gamma_H = \frac{U_H - (U_B + U_{\text{H}_2\text{O}(l)})}{A} \quad (5)$$

where U_H is now the energy of the hydrated surface block and $U_{\text{H}_2\text{O}(l)}$ is the energy of bulk water, which is the sum of the self-energy of water, described above, and the energy of condensation of water (-44 kJ mol^{-1} [47]).

3. Results and discussion

3.1. DFT calculations

α -Quartz has a hexagonal structure with spacegroup $P3_121$ and a unit cell of $a = b = 4.91 \text{ \AA}$, $c = 5.41 \text{ \AA}$ and $\alpha = \beta = 90^\circ$ and $\gamma = 120^\circ$ [48]. In the DFT calculations, upon electronic and geometry optimization, these lattice parameters contracted somewhat to $a = b = 4.85 \text{ \AA}$, $c = 5.30 \text{ \AA}$, but the calculated a/c parameter at 0.91 agrees

to within 0.9% with the experimental value. We used two different terminations of the (0001) surface as starting configurations for our calculations, one plane where the bulk material was simply cleaved to give an (0001) surface with under-coordinated Si and O species (Fig. 1a and b), and one (0001) plane where the under-coordinated surface species regained their bulk coordination by the formation of O–Si–O silanol bridges in the surface (Fig. 1c and d) [15]. Both surfaces were then fully electronically and geometry optimized before calculating the surface energies of the two surfaces. When optimized, the bulk-terminated surface simply relaxed to a lower energy structure, still with under-coordinated surface silicon atoms and oxygen dangling bonds. However, the case was less simple for the fully coordinated surface. This surface, where the oxygen dangling bonds are combined with the under-coordinated surface silicons to form four- and two-coordinated surface silicon and oxygen atoms respectively, was obtained spontaneously during geometry optimization of the bulk-terminated plane in interatomic potential-based simulations [15]. As such we were interested to calculate whether this termination of the {0001} surface is energetically more favourable than the surface with dangling bonds. We therefore relaxed a bulk-terminated slab in potential-based simulations and used the final surface structure as the starting configuration of our electronic structure calculations of the fully coordinated surface slab, which was then fully electronically and geometry optimized. We hence had obtained two fully optimized slabs with different surface terminations, as shown in Fig. 1, for comparison of the relative stabilities and reactivities towards water.

We first determined the surface energies for the dry surfaces, which were calculated to be 0.91 J m^{-2} for the fully coordinated plane and 2.28 J m^{-2} for the under-coordinated (0001) surface with dangling bonds, respectively. Clearly the fully coordinated (0001) quartz surface (Fig. 1c and d) has a much lower surface energy than the under-coordinated surface (Fig. 1a and b), which is thus a local minimum energy structure rather than the lowest energy configuration of the anhydrous quartz surface, and the fully coordinated surface

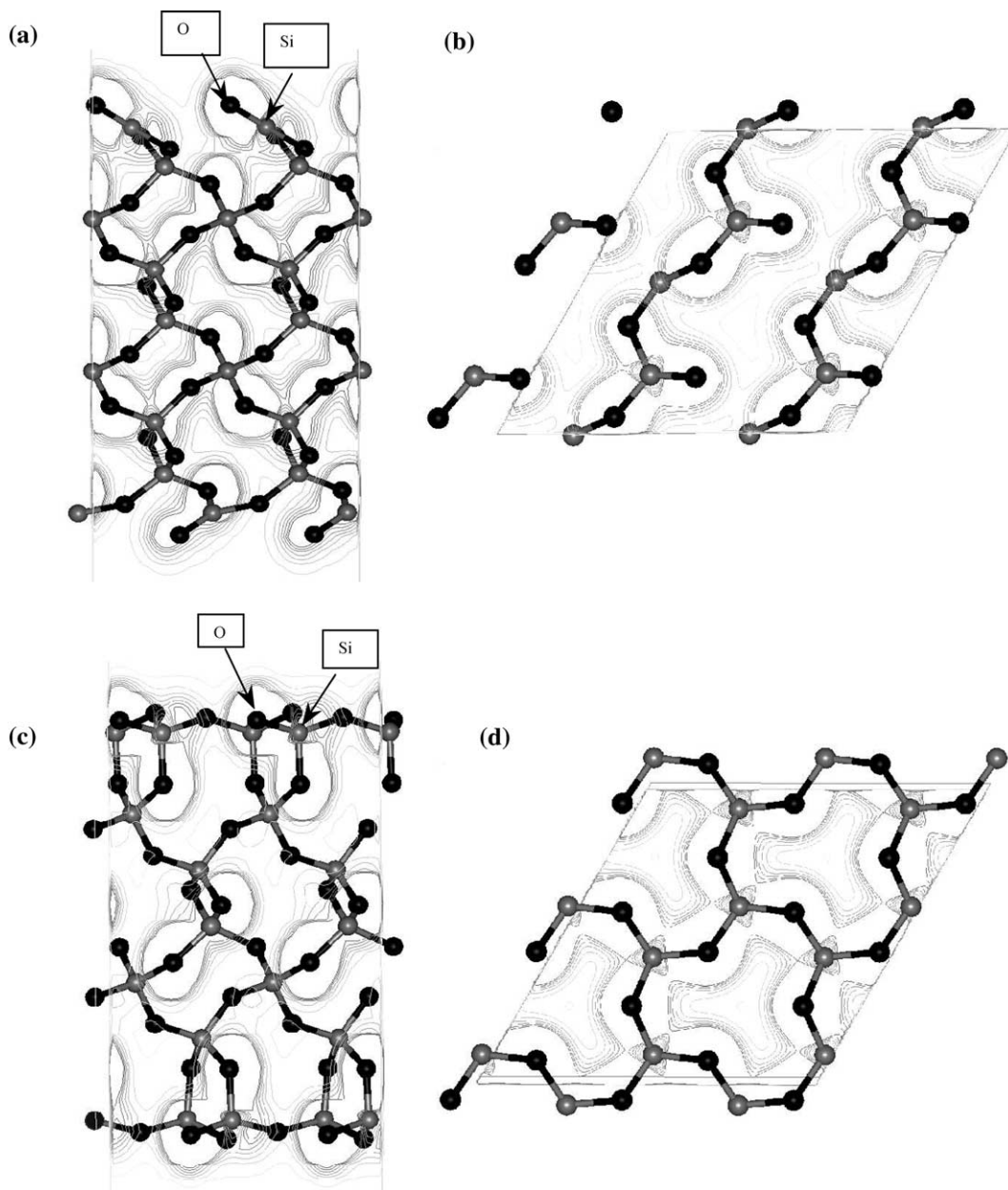


Fig. 1. Side (a) and top (b) views of the geometry optimized under-coordinated (0001) surface, and side (c) and top (d) views of the geometry optimized fully coordinated (0001) surface, showing electron density contour plots through planes containing surface Si and O as indicated on the side views, (a) and (c), and through the top silicon layer, (b) and (d) (Si = gray, O = black, contour levels from 0.02 to 0.26 eÅ⁻³ at 0.04 eÅ⁻³ intervals).

with the silanol bridges is the more stable structure. The fully coordinated surface was first identified to be the preferred and spontaneously formed termination of the quartz (0001) surface

in earlier work, using interatomic potential-based energy minimisation methods [15], which was later confirmed by ab initio molecular dynamics simulations by Koudriachova et al. who started from

an under-coordinated surface which reconstructed into the lower-energy fully coordinated surface upon heating over 400 K [49]. Rignanese and co-workers also used ab initio molecular dynamics methods to investigate the α -quartz (0001) surface, but they did not study the same surface terminations. They did investigate the same under-coordinated surface, but constructed a different fully coordinated surface with edge-sharing SiO_2 groups, which was however unstable upon relaxation and energetically less favourable than the under-coordinated surface, forming one four-coordinated silicon bonded to an oxygen dimer and a two-coordinated silicon at the surface [18]. We obtained a similar surface from one of our calculations, but like Rignanese and co-workers' surface this plane was not stable. However, they also identified an alternative surface, which does contain four-coordinated silicon and two-coordinated oxygen species and which is more stable than either the under-coordinated or the dimer surface, although it is a highly reconstructed and dense surface and not comparable to the fully coordinated surface described here or in Refs. [15,49].

The optimized geometrical parameters of the two surfaces together with the geometries of the bulk-terminated surface before relaxation are presented in Table 2. Upon optimization, the Si–O bond lengths between the surface silicon and oxygen atoms in the fully coordinated surface are only slightly longer than those at the bulk-terminated surface. Similarly, the O–Si–O angles are close to the tetrahedral angles found in the bulk material. However, the Si–O–Si angles at the fully coordinated surface are smaller than the bulk value due to the formation of the O–Si–O bridges at the surface, which are in the same layer of the (0001) plane and more horizontal than in the

bulk material, where bridges are formed to oxygen and silicon atoms in different layers more perpendicular to the (0001) plane (Fig. 1c). At the under-coordinated surface terminated with dangling bonds, the Si–O bond lengths are significantly shorter than in the bulk. These bonds have contracted due to the under-coordination of the surface species, which is a general phenomenon in surfaces where the breaking of bonds at the surface results in a contraction of surface species into the bulk material, for example in α -alumina [50,51]. Both Si–O–Si and O–Si–O angles have diverged from those in the bulk material, due to the strong relaxation of the surface region.

Side and plan views of the relaxed structures of the two α -quartz (0001) planes are shown in Fig. 1, together with electron density contour plots (through the planes containing species indicated by arrows). These contour plots show that in all cases there is a significant distribution of the electron density along the Si–O bonds, both at the surfaces and in the bulk, indicating that the Si–O bond is not fully ionic but has a degree of covalency. From the side views in Fig. 1(a) and (c) we see that in the fully coordinated surface (Fig. 1c), the silicon and oxygen atoms of the second layer have moved up into the first layer to form the horizontal silanol bridges. Fig. 1(d) shows a top view of this layer only with the electron density plot through the plane of the silicon atoms. The figure shows that the surface Si and O species form almost planar six-rings in the top layer, and that electron density of up to $0.26 \text{ e}\text{\AA}^{-3}$ is distributed along the Si–O bonds in a continuous network parallel to the surface. In the under-coordinated surface, however, despite contraction of the surface region as a whole, the second layer oxygen and silicon atoms have remained at different heights in the surface (Fig. 1a), without

Table 2

Structural parameters of the unrelaxed bulk-terminated surface compared to the relaxed fully coordinated and under-coordinated dry surfaces (bond lengths in Å and bond angles in degrees)

	Bulk-terminated	Fully coordinated	Under-coordinated
Si–O	1.63, 1.59	1.63, 1.62, 1.61	1.65, 1.56, 1.46
\angle O–Si–O	112.3, 109.5, 107.3	111.8, 111.2, 108.2, 107.9	127.6, 126.4, 106.0
\angle Si–O–Si	139.1	123.0, 120.2, 116.3	144.0, 125.9

the formation of a closed ring structure and no continuous network of electron density is found in the surface layer (Fig. 1b).

3.1.1. Adsorption of water

We next introduced water molecules onto the two quartz surfaces. We first calculated adsorption of molecular water at the fully coordinated α -quartz surface, where we investigated a large number of initial configurations of the water molecule. In the starting configuration leading to the lowest energy structure, the oxygen atom of the water molecule is attached to the surface silicon atom with a Si–O_{water} distance of about 2.0 Å and distances between the hydrogen atoms of the water molecule and surface oxygen atoms of about 2.23 Å. The water molecule is initially located perpendicular to the surface with both hydrogen atoms of the water pointing away from the quartz surface, but after electronic and geometry optimization, the resulting structure (Fig. 2) shows that at the fully coordinated α -quartz surface the water molecule

rotates to lie almost flat upon the surface but does not dissociate upon adsorption. The water molecule remains associatively adsorbed with Si–O_w and O–H_w distances of 3.11 and 2.33 Å respectively. The electron density contour plot through a plane containing a surface silicon atom (and oxygen) as well as the water molecule's oxygen atom (Fig. 2a) shows that the electron density is mainly centered on the ions and there is no significant electron density distribution along the Si–O_w axis, indicating that the Si–O_w interaction is distinctly different from the Si–O bonds in the crystal. In Fig. 2(b) an electron density contour plot through a plane containing a surface oxygen and one hydrogen of the water molecule is shown, where some charge density is distributed along the O–H axis (up to 0.07 eÅ⁻³) indicating weak hydrogen-bonding by the water molecule to the surface oxygen. No formal chemical bonds have formed between the surface and water molecules and the adsorption appears to be associative physisorption with hydrogen-bonding between hydrogen and

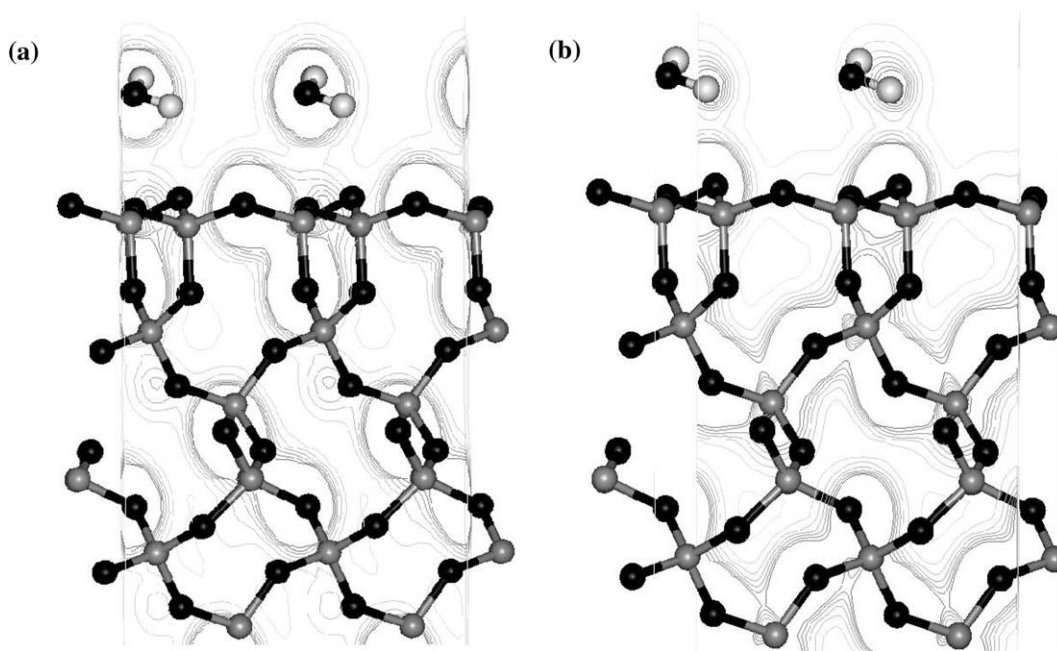


Fig. 2. Geometry optimized structure of the fully coordinated (0001) surface slab with associatively adsorbed water molecules, showing electron density contour plot through planes containing (a) both a surface silicon atom and the oxygen atom of the water oxygen, and (b) a surface oxygen atom and one of the hydrogen atoms of the water molecule (Si = gray, O = black, H = white, electron density contour levels from 0.02 to 0.22 eÅ⁻³ at 0.04 eÅ⁻³ intervals).

surface oxygen. We investigated whether dissociation of the water molecule would be energetically preferred but hindered by an activation energy, by adsorbing dissociated water molecules at the surfaces, i.e. attaching a hydroxy group to a surface silicon atom and a hydrogen atom to a surface oxygen atom, before allowing the system to optimize. However, the initially dissociated surface OH groups recombined to form associated water molecules, hence clearly showing that associative adsorption is the preferred mode of adsorption of water at the fully coordinated (0001) surface. This molecular adsorption is an exothermic process releasing 45.3 kJ mol^{-1} , which relatively small hydration energy also indicates the weak physisorption of the water at the surface.

We next investigated the adsorption of water molecules at the under-coordinated (0001) surface. Upon full electronic and geometry optimization, the water molecule dissociated, with the formation of two OH groups on the surface (Fig. 3), indicating that there is no significant energy barrier to the dissociation of a water molecule. It is clear from Fig. 3, showing electron density contours through the plane of surface silicon atoms and the oxygen atoms of the hydroxy groups, that significant electron density is distributed along the Si–OH bond indicating covalent character just like the Si–O bonds in the silicate structure. Likewise, the O–H bond is also semi-covalent as is evident from the electron density contour plot through the O–H plane in the hydroxy groups, which is similar to OH groups in other materials [52]. In addition, Fig. 3 shows that there is also electron density distributed between the hydrogen of one hydroxy group to the oxygen of the second group, indicating hydrogen-bonding between the hydroxy groups. This dissociative chemisorption, terminating the dangling bonds of the under-coordinated Si and O species by OH groups is far more exothermic than the molecular adsorption at the fully coordinated surface described above with an adsorption energy of $-140.7 \text{ kJ mol}^{-1}$. The higher reactivity of the under-coordinated surface towards water is most likely due to termination of the dangling bonds, where the hydrated surface now contains only fully coordinated surface species. The same preference by under-coordinated

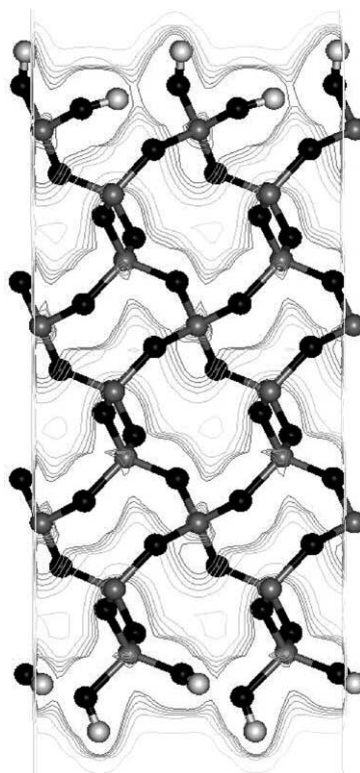


Fig. 3. Geometry optimized structure of the under-coordinated (0001) surface slab with dissociatively adsorbed water molecules terminating the dangling bonds, showing electron density contour plot through a plane containing a surface silicon atom (Si = gray, O = black, H = white, electron density contour levels from 0.02 to $0.22 \text{ e}\text{\AA}^{-3}$ at $0.04 \text{ e}\text{\AA}^{-3}$ intervals).

species on silicate surfaces to be capped by hydroxy groups was shown in interatomic potential-based calculations of quartz and vitreous silica surfaces [15,22]. If the water had adsorbed in a molecular fashion, the surface Si and O atoms would have remained under-coordinated, which as we saw for the anhydrous surfaces is a highly unstable configuration. Termination of the dangling bonds and hence increasing the coordination of the surface species is thus the driving force behind the dissociation of the adsorbed water molecules, aided by the formation of the residual hydrogen-bonding between the hydroxy-groups which further stabilises the hydrated surface.

The calculated surface energies of the hydrated surfaces are now 1.08 J m^{-2} for the hydrated fully

coordinated (0001) surface and 0.12 J m^{-2} for the hydrated (formerly) under-coordinated surface respectively. In the case of the fully coordinated surface, the stability of the surface has decreased upon hydration as shown by the increased surface energy. This decreased stability is probably due to the fact that the dry surface is already a stable plane where all surface species have their bulk-coordination numbers. Addition of the adsorbed water molecules only serves to make the surface less smooth, and disrupts the network of electron density along the planar six-rings in the surface, leading to the decrease in stability. Conversely, for the under-coordinated surface, the surface energy of the hydrated surface is much smaller than that of the dry surface and this plane has now become the preferred termination of the (0001) surface. The reason for this stability lies in the structure of the hydrated surface. The oxygen atoms of the hydroxy groups that become attached to the surface silicon atoms, fill positions on the surface that would be taken by oxygen atoms in the silica lattice if a new layer of material was grown on the surface, which can be seen in Fig. 3 if we compare the SiO_4H_2 groups at the surfaces with the equivalent SiO_4 groups in the bulk material. The hydrogen atoms complete the coordination of the surface oxygen atoms and to a certain extent mimic bulk Si atoms by bridging to a second oxygen through hydrogen-bonding.

3.2. Interatomic potential-based simulations

The accuracy of potential-based simulations is largely dependent on the quality of the interatomic parameters. In the simulations, we have used the SiO_2 potential model of Sanders et al. [11], the Si–OH parameters optimized by Baram and Parker [44] and the water potential model by de Leeuw and Parker [45]. A similar combination of these potential models has previously been used successfully in a study of hydration of quartz surfaces [15], but we decided to repeat the DFT calculations using the same simulation cell to gain information on the agreement or discrepancy between the methods. In all cases, the thickness and the gap width of the surfaces as well as the initial position of the water molecule is the same as that in the

DFT calculations, unlike the simulations in Ref. [15].

At the fully coordinated surface, associative adsorption of the water molecules was preferred similar to the DFT calculations. Using the potential model from Ref. [15], the energy of adsorption was calculated to be $-105.1 \text{ kJ mol}^{-1}$ and the Si– O_{water} distance was found to be 1.79 \AA , indicating that the surface silicon atom has now become coordinated to five oxygen atoms, which is clearly unrealistic. Compared to the DFT calculation of the same system, both the structure and hydration energy of the potential-based simulation indicates that the interaction between the water molecule and the surface is too strong. However, a minor refinement of the potential between the silicon atom and oxygen atom of the water, gave a much closer agreement between the two methods. The A parameter of the Buckingham potential between Si and O_{water} was adjusted to the value in the Si– $\text{O}_{\text{hydroxy}}$ potential, which parameter had been carefully fitted to experimental hydroxide structures and hence presented a suitable, well-tested alternative for the Si– O_{water} potential [44]. The energy of the hydration process is now calculated at $-56.9 \text{ kJ mol}^{-1}$, which at a difference of 11.6 kJ mol^{-1} is in acceptable agreement with the DFT calculation. The distance between the water oxygen atom and the surface silicon and the distance between hydrogen atom and surface oxygen atom are 2.82 and 2.08 \AA respectively compared to 3.11 and 2.33 \AA for the equivalent DFT calculation. Although the water molecule in the potential-based simulation is still adsorbed more strongly to the surface, the agreement between the methods is acceptable taking into account the necessary approximations employed in both methods, for example, the fact that full charges are used in the SiO_2 potential model and the use of the generalized gradient approximation in the DFT calculations, which usually underestimates the strength of chemical bonding. Instead of, or in addition to, adjusting the Si– O_{water} parameters, we could also have refined the $\text{O}_{\text{surface}}\text{--}\text{O}_{\text{water}}$ potential, which would also have had a significant effect on both hydration energies and adsorption structures. However, the $\text{O}_{\text{surface}}\text{--}\text{O}_{\text{water}}$ potential parameters were derived in previous simulations of the

hydration of surfaces of MgO [53] and have since been used in many other studies of different oxides, including CaO, Fe₂O₃ and Al₂O₃ e.g. [54,55], where they have been shown to agree well with both experiment and results from electronic structure calculations. As such, we decided not to alter these potential interactions, but to concentrate on the Si–O_{water} parameters, which have been used to a lesser extent in previous simulations and which gave the required adjustment to the hydration structures and energies.

At the under-coordinated surface, adsorption of dissociated water released 213.7 kJ mol⁻¹. In this case the energy difference between the two methods is fairly large at about 73 kJ mol⁻¹. However, despite the discrepancies between the two methods in the latter calculation, we were reluctant to adjust the potential parameters of the hydroxy group. As already mentioned in the previous paragraph, the potential model for hydroxy groups in silicate materials was carefully derived and tested, using several quantum mechanical and experimental data [44], and, moreover, the calculated value of 213.7 kJ mol⁻¹ for dissociative adsorption of water at the (0001) surface using the interatomic potential method agrees very well with

experimental temperature programmed desorption measurements by Fubini et al. [56], who measured adsorption energies of approximately –200 kJ mol⁻¹ for dissociative adsorption at the quartz surface. As such we consider that the potential model listed in Table 1 is in good agreement with experiment and sufficiently reliable to be used in our further study of the hydration of a silicate nano-tube.

3.2.1. Hydration of a silica nano-tube

The model silica nano-tube we have chosen to study is a short tube consisting of 36 SiO₂ units, leading to simulation cells of between 180 and 200 species for the anhydrous and hydrated tubes respectively. The nano-tube is constructed out of six hexagonal planar six-membered rings, each containing six silicon and six oxygen atoms (Fig. 4a) and these interior rings are linked to each other by six bridging oxygen atoms, hence forming a network of corner-sharing SiO₄ tetrahedra. In order to retain stoichiometry, the end rings are capped at both ends by three oxygen atoms rather than six, leading to rings with alternating fully four-coordinated Si atoms and three-coordinated Si atoms. The three final oxygen atoms also have

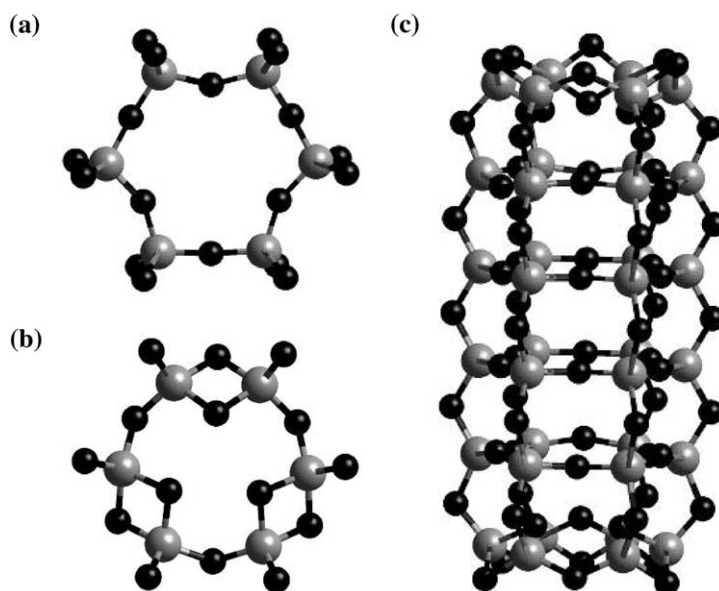


Fig. 4. Geometry optimized structure of (a) interior layer, (b) end layer and (c) complete SiO₂ nano-tube (Si = gray, O = black).

dangling bonds, being only coordinated to one silicon atom each. When the structure is geometry optimized, these three oxygen atoms spontaneously relax to form bridges to the three-coordinated Si atoms, leading to alternating single and double oxygen-bridges between the silicon atoms, even though this entails the formation of strained edge-sharing SiO_4 tetrahedra (Fig. 4b). The resulting structure is a stoichiometric silica nano-tube with the bulk built up of corner-linked SiO_4 tetrahedra, where all Si and O atoms are four- and two-coordinated respectively (Fig. 4c), but capped by three single and three double oxygen-bridges at each end. The size and geometry of the nano-tube rings are similar to the channels in α -quartz or the six-rings in microporous silicate materials, such as zeolites, and the outer wall of the tube resembles the anhydrous fully coordinated α -quartz (0001) surface described above. Moreover, the hexagonal six-rings of the nano-tube structure exist in natural cyclo-silicate materials such as beryl, which contains columns formed of rings consisting of six SiO_4 tetrahedra linked by Be and Al ions, where interstitial species such as water molecules and foreign cations are found in the channels [47]. The lattice energy of the nano-tube per SiO_2 unit is within approximately 0.5 eV of the average lattice energy per SiO_2 unit in the thin slab of α -quartz above, indicating that the two silica structures are of comparable stability. In addition to the present study, thin slabs of silicate and other materials are routinely used in computational studies to model surface structures and processes e.g. [18,57] while cluster models are often used to study reactive sites and defects in extended silicate systems (e.g. [9]). Such calculations have been found to give reliable and accurate results and we thus consider that our silica nano-tube structure is a viable model for nano-particulate silicate, which will give insights into the reaction of water with strained Si–O bonds in silica nano-particles. Similar to the simulations of the surface slabs described above, the nano-tube was modelled in a simulation cell employing three-dimensional periodic boundary conditions. The size of the cell was $100 \text{ \AA} \times 100 \text{ \AA} \times 100 \text{ \AA}$, which ensured that there would be no interactions between the nano-tube and its images.

We first investigated the energies of adsorption of associated water molecules to a variety of sites on the SiO_2 nano-tube. Again, a large range of possible starting configurations was sampled to ensure that upon relaxation the true lowest energy position rather than a local minimum was obtained. As such, initial configurations of the water molecules included adsorbing them by their oxygen atom to Si sites and by their hydrogen atom to oxygen atoms on the tube wall. We found, however, that even when the water molecule was initially positioned with its hydrogen atoms directed towards surface oxygen atoms and its oxygen atom pointing away from the tube side, the Si– O_{water} interactions were sufficiently large that in the final position the water molecule also coordinated through its oxygen atom to one or two surface silicons, at about 2.76 Å at the wall of the tube (Fig. 5a) and 2.30 Å at the end, while hydrogen-bonding to surface oxygen atoms at 1.85–2.16 Å. This type of associative physisorption of molecular water, without the formation of a Si– O_{water} chemical bond, is similar to that observed on the fully coordinated quartz (0001) surface above. In addition, this preference for interaction of the water molecule's oxygen atom with the cation, rather than hydrogen-bonding to surface oxygen atoms is also seen in ionic or other semi-covalent systems, where both quantum mechanical calculations and atomistic simulations identified the cation–oxygen interaction as the major adsorption feature when water adsorbed in a molecular fashion [13,58,59]. Although it is not possible to separate completely the Si– O_{water} and H– O_{tube} interactions for the adsorbed water molecules, we can quantify the Si– O_{water} interaction to some extent by way of the hydration energies given in Table 3. For the potential model used for the water molecule in this study, the formation of a single hydrogen-bond of 1.8 Å releases 20.2 kJ mol^{-1} , which agrees well with the experimental value of 22.1 kJ mol^{-1} [60]. At the end ring, where the Si– O_{water} interaction is the more significant, the adsorbed water molecule forms one hydrogen-bonded interaction to a surface oxygen atom at 1.85 Å, which should hence release approximately 20 kJ mol^{-1} . The energy released upon hydration is $-63.4 \text{ kJ mol}^{-1}$ and the Si– O_{water} interaction thus

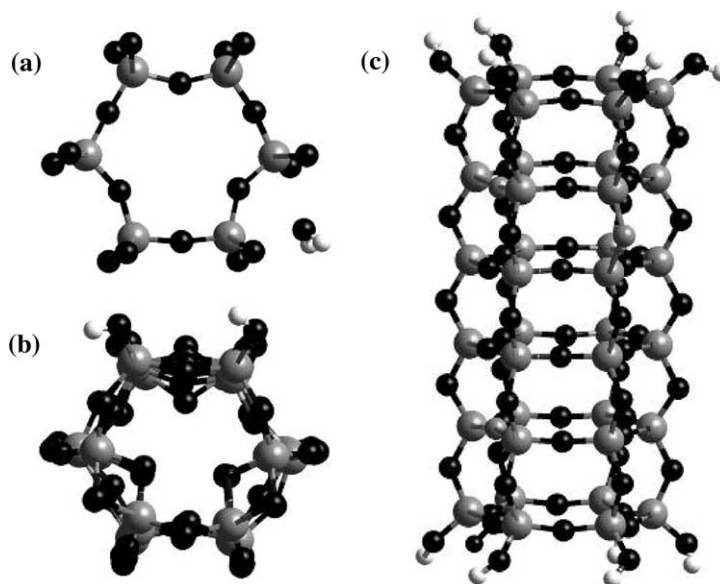


Fig. 5. Geometry optimized structure of the SiO₂ nano-tube with (a) an associatively adsorbed water molecule at the side of the tube, (b) a dissociated water molecule at the end of the tube and (c) with three dissociated water molecules adsorbed at the two end rings leading to a fully hydrogen-capped nano-tube structure (Si = gray, O = black, H = white).

Table 3

Hydration energies of associated and dissociated water at different surface sites of the silicate nano-tube (in kJ/mol)

Position	Associated	Dissociated
End Si	-63.4	-511.3
Wall Si	-45.5	-81.2

accounts for a maximum of approximately 43 kJ mol⁻¹, which is more than the energy of two H–O_{tube} hydrogen-bonds and is thus clearly the preferred interaction between the water molecule and the silica nano-tube, especially as the water molecule can form additional hydrogen-bonds to the nano-tube as well as the Si–O_{water} interaction. The hydration energies are similar for adsorption at silicon atoms on the side or at the end of the tube, although adsorption at the end of the tube is preferred by about 18 kJ mol⁻¹.

We next adsorbed dissociated water at the different sites, where the OH group was adsorbed to a surface silicon atom and the proton to a neighbouring oxygen atom, which leads to the breaking of a Si–O bond in the nano-tube. Again, all possible starting configurations were investigated.

From the hydration energies in Table 3 we see that dissociative adsorption of water at the nano-tube wall is more favourable than associative adsorption at the same site by 35.7 kJ mol⁻¹. However, this difference in energy is sufficiently small that the driving force to dissociation of the associatively adsorbed water molecule will be small, especially taking into account the low energy of dissociative adsorption which at 81 kJ mol⁻¹ is more in the realm of physisorption than chemisorption. In addition, substantial kinetic energy barriers to dissociative adsorption will also be expected. For example, breaking the Si–O bond in the diatomic SiO molecule costs approximately 800 kJ mol⁻¹ and even though this process will probably be significantly less endothermic in an extended system like the nano-tube, where each silicon forms four Si–O bonds, it will still be a formidable energy barrier to overcome. Associative rather than dissociative adsorption would also agree with the same process in both bulk α -quartz, where electronic structure calculations have shown that interstitial water remains a molecular species [13], and our DFT calculations of the fully coordinated (001) surface described above. In

addition, the atomistic adsorption energy for dissociative adsorption may be overestimated to some extent, as was shown by comparison with the DFT results.

Dissociative adsorption of water at an end silicon atom, leading to two vicinal hydroxy-groups at the end of the nano-tube (Fig. 5b), releases a very large hydration energy, 511 kJ mol^{-1} which is clearly in the realm of dissociative chemisorption and in excess of the adsorption energies found for even the most reactive of quartz surfaces ($<465 \text{ kJ mol}^{-1}$) [15]. The two vicinal hydroxy groups replace one of the two double oxygen bridges between two Si atoms leading to normal tetrahedral O–Si–O angles for these two silicon atoms and corner-sharing rather than edge sharing SiO_4 units. The resulting structure is thus less strained than the original anhydrous nano-tube, leading to the release of this large amount of energy. Although the Si–O bond lengths in the relaxed nano-tube at 1.59 – 1.70 \AA resemble bulk quartz (1.61 \AA), the Si–O–Si angles in the middle of the nano-structure at 152° – 176° are larger than in bulk quartz (141.3°) whereas in the single oxygen-bridges of the end-ring they are smaller by about 15° . However, it is the divergence of the O–Si–O and Si–O–Si angles in the double oxygen-bridges within the end rings away from the equilibrium angles of bulk quartz to very small angles of as low as 83° and 95° – 118° respectively, which cause the strain in the end-ring structure. Even though the double oxygen bridges formed spontaneously upon energy minimisation and are stable with respect to under-coordinated Si and O species at the end of the tube, dissociative adsorption of water at the end-ring breaks one of these double Si–O–Si bridges, leading to normal tetrahedral O–Si–OH angles, with the consequent release of very large hydration energies suggesting that the oxygen atoms of the end ring would prefer to be capped by hydrogen atoms rather than O–Si–O bridges.

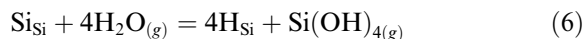
We next calculated the formation of two isolated hydroxy-groups on both the end and the wall of the nano-tube, which would give an indication of the likelihood of surface diffusion of the hydroxy-groups on the nano-tube. On the wall, the formation of isolated hydroxy groups is an

increasingly endothermic process costing from 104 to 186 kJ mol^{-1} , for positions from two to six sites apart as low-coordinated surface species are created and hydrogen-bonded interactions between the two OH groups are lost as the distance between them increases. It is clear from these energies that even if water were to be dissociatively adsorbed at the tube wall, we can expect no significant surface diffusion of the adsorbed hydroxy groups away from the vicinal positions. On the end sites, formation of hydroxy-groups two sites apart which also led to the split of only one double oxygen-bridge had little effect on the hydration energy (-501 kJ mol^{-1}), but when the hydroxy groups were fully isolated on either side of the end ring, the process was much less exothermic at -352 kJ mol^{-1} . In this case the attachment of the hydroxy-group to a silicon atom also leads to the fracture of one of the double oxygen-bridges but with the formation of an under-coordinated ring oxygen and hence a dangling bond, which was no longer capped by a proton. This is a much less stable structure, hence leading to the smaller hydration energy. Finally, we fully hydrated the two end rings by dissociated water molecules, three at each ring, to investigate whether the nano-tube structure is preferentially terminated by complete oxygen-rings (containing six instead of three oxygen atoms) which are all capped by hydrogen atoms to remove the dangling bonds of the terminating oxygen atoms, rather than forming double oxygen-bridges between the end silicon atoms. The calculated process is equal to adding three water molecules to each end ring according to Eq. (1). The average hydration energy released in this process is calculated at $-472.9 \text{ kJ mol}^{-1}$ per water molecule and it is thus clear that this hydrogen-capped structure will be the preferred state of the silica nano-tube (Fig. 5c).

3.2.2. Dissolution of the nano-tube

Our results so far show that the end rings of the silica nano-tube will be fully hydrated by dissociatively adsorbed water molecules, leading to an unstrained structure where the end oxygen rings are capped by hydrogen atoms. However, we are also interested to see whether hydration of the end of the tube will progress beyond a fully protonated

end-ring and hence lead to dissolution of the nano-tube. We therefore investigated the sequential dissociative adsorption of four water molecules to one silicon atom at the end ring of the nano-tube with the formation of two geminal hydroxy groups and eventual dissolution of this Si atom and its replacement by four protons according to the process in Eq. (5):



where Si_{Si} is a silicon atom at a silicon site in the nano-tube and H_{Si} is a proton adsorbed at a silicon site. This process, which is a well-known defect structure in many silicate materials, was calculated to be energetically favourable in bulk α -quartz [13]. For the sake of completeness, we have calculated this dissolution of an end silicon atom for both the anhydrous and hydrogen-capped structures, to evaluate whether the presence of the remaining double oxygen bridges in the anhydrous tube makes a difference to the dissolution energies.

Table 4 shows the energies released when consecutive dissociated water molecules are adsorbed to one silicon in an end-ring, where addition of each water molecule adds another OH group to

Table 4

Sequential energies of dissociative hydration of the end rings of the nano-tube for the anhydrous and fully hydrogen-capped structures, leading to dissolution of one silicon atom

Number of water molecules	Anhydrous structure	Hydrogen-capped structure
1	-511.3	-
2	-133.0	-43.3
3	-42.7	-41.2
4	+11.6	+24.6

the silicon and a proton to a neighbouring oxygen. Eventually, the silicon atom is bonded to four OH groups and is detached from the nano-tube, where the vacancy remaining behind is surrounded by four OH groups. The two structures are shown in Fig. 6, from which we see that the structure of the defect is similar for both tube structures. However, unlike the same defect in bulk quartz, the four protons are not pointing towards the silicon vacancy but two are angled away from the vacancy, to retain the tetrahedral O–Si–OH angles. We see from Table 4 that addition of the first three water molecules is exothermic for both structures, although the addition of the second dissociated

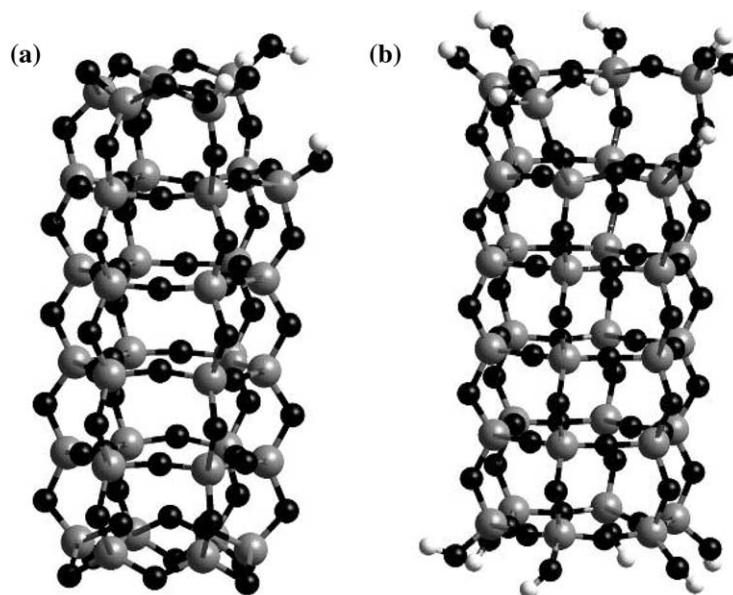


Fig. 6. Geometry optimized structures of (a) the anhydrous SiO_2 nano-tube with one end silicon atom replaced by four protons and (b) the hydrogen-capped nano-tube also with one Si dissolved from the structure (Si = gray, O = black, H = white).

water molecule to the anhydrous structure releases about three times as much energy as addition to the hydrogen-capped structure. Again, this effect is due to the strained structure of the anhydrous tube, where after the breaking of one of the three double oxygen bonds by the first water molecule, the addition of a second water molecule breaks one of the single oxygen bridges, hence opening up the end-ring structure and enabling the neighbouring SiO_4 unit to rotate into a more favorable configuration, even though it is still attached by a double-oxygen bridge to the next silicon. Addition of the third water molecule does not have much effect on the anhydrous structure and the energies of the two nano-tube structures are hence very similar. Addition of the fourth water molecule with the formation of the $\text{Si}(\text{OH})_4$ species is less straightforward. If the $\text{Si}(\text{OH})_4$ species remains closely associated with the nano-structure through hydrogen-bonding, the process is just endothermic (Table 4). On the other hand, if the $\text{Si}(\text{OH})_4$ molecule is removed infinitely far from the now defective nano-structure, the last step becomes much more endothermic, 69 kJ mol^{-1} for the anhydrous structure and 51 kJ mol^{-1} for the hydrogen-capped structure, and the $\text{Si}(\text{OH})_4$ molecule is thus unlikely to become completely detached from the nano-tube. However, both anhydrous and hydrogen-capped nano-tubes are clearly amenable to significant disruption and fragmentation of their structure by water, even though they are marginally resistant towards complete dissolution of silicon atoms in the end rings.

4. Conclusion

Accurate DFT calculations as well as computationally less expensive interatomic potential-based simulations have been employed to study the structures and stabilities of two silicate surfaces and a silicate nano-tube and their affinity for water. Our calculations show that of the two anhydrous quartz surfaces, the fully coordinated (0001) surface containing surface O–Si–O bridges and planar six-rings is more stable than the under-coordinated surface where the surface silicon and

oxygen atoms are terminated by dangling bonds. Upon hydration, these stabilities are reversed with the formerly under-coordinated surface, where the dangling bonds are now terminated by OH groups, by far the more stable of the two. We would therefore suggest that under ultra-high vacuum conditions, the fully coordinated surface would be formed whereas in the presence of water the hydroxylated surface would be dominant.

Associative physisorption of water occurs on the fully coordinated surface with a decrease in stability of the surface, whereas dissociation of water leading to a fully hydroxylated surface is the preferred mode of adsorption at the dangling bonds of the under-coordinated surface, hence increasing the coordination and local geometry of the surface species to resemble a bulk-like environment. A similar trend is shown in the hydration calculations of the silica nano-tube, where the tube walls containing fully coordinated species linked by O–Si–O bridges are fairly resistant towards attack by water, as the non-destructive associative physisorption of water is unlikely to be followed by dissociative adsorption with consequent breaking of Si–O bonds, which is energetically not much more favourable.

However, the atoms at the end of the nano-tube are highly reactive towards water, not only initially due to the strained environment of the end-ring in the anhydrous tube, but the structure is easily destroyed even further by dissociative chemisorption of water and possibly replacement of silicons by protons, even though the final Si–O bond, which links the silicon atom in the end ring to the oxygen atom bridging to the next six-ring, is thermodynamically just stable against dissolution by dissociative water. From our calculations it is clear that long nano-tubes or closed structures will be significantly more resistant against dissolution than short open-ended structures. As the ends of the nano-tube are only meta-stable in the presence of water, synthesis of this structure will be a challenge for experimental solid state chemists. ‘Chemical gardens’ have been used to grow nanometer-sized rods of almost pure silica [61,62]. These rods are found to grow very fast to form long tubes, which self-assemble into second order structures [58]. This fast growth from the uncapped rod ends into

long, un-branched tubes shows that silica nano-tubes are indeed reactive at the open end structure, but stable at the sides, in agreement with our calculations described in this work.

The work described in this paper, showing the interplay between electronic structure calculations and potential-based techniques, is a clear example of the benefits derived in employing complementary methods to identify and investigate important surface features and reactivities. Future work will include calculations of the adsorption of second and further water layers at the dry and hydroxylated surfaces to study the effect of the presence of the oxide surface on the structure of bulk water, and molecular dynamics simulations to investigate the effect of temperature on the hydration and dissolution behaviour of the nano-tube structures. In addition, we intend to investigate the assembly of a collection of single nano-tubes into two- and three-dimensional arrays.

Acknowledgements

We thank the Natural Environment Research Council, grant no. NER/T/S/2001/00855, for financial support under their E-science initiative and NHdL thanks EPSRC for an Advanced Research Fellowship.

References

- [1] M. Niederberger, M.H. Barti, G.D. Stucky, *J. Am. Chem. Soc.* 124 (2002) 13642.
- [2] N. Nishiyama, S. Tanaka, Y. Egashira, Y. Oku, K. Ueyama, *Chem. Mater.* 15 (2003) 1006.
- [3] M.P. Zach, J.T. Newberg, L. Sierra, J.C. Hemminger, R.M. Penner, *J. Phys. Chem. B* 107 (2003) 5393.
- [4] H.-F. Zhang, C.-M. Wang, E.C. Buck, L.-S. Wang, *Nano Lett.* 3 (2003) 577.
- [5] J.F. Bertone, J. Cizeron, R.K. Wahi, J.K. Bosworth, V.L. Colvin, *Nano Lett.* 3 (2003) 655.
- [6] D.T. Mitchell, S.B. Lee, L. Trofin, N. Li, T.K. Nevanen, H. Söderlund, C.R. Martin, *J. Am. Chem. Soc.* 124 (2002) 11864.
- [7] D.T. Griggs, J.D. Blacic, *Science* 147 (1965) 292.
- [8] T. Reuschle, M. Darot, *Eur. J. Mineral.* 8 (1996) 695.
- [9] J. Purton, R. Jones, M. Heggie, S. Oberg, C.R.A. Catlow, *Phys. Chem. Miner.* 18 (1992) 389.
- [10] R. Jones, S. Oberg, M.I. Heggie, P. Tole, *Philos. Mag. Lett.* 66 (1992) 61.
- [11] M.J. Sanders, M. Leslie, C.R.A. Catlow, *Chem. Commun.* (1984) 1271.
- [12] R. Nada, C.R.A. Catlow, R. Dovesi, C. Pisani, *Phys. Chem. Miner.* 17 (1990) 353.
- [13] N.H. de Leeuw, *J. Phys. Chem. B* 105 (2001) 9747.
- [14] O. Sneh, S.M. George, *J. Phys. Chem.* 99 (1995) 4639.
- [15] N.H. de Leeuw, F.M. Higgins, S.C. Parker, *J. Phys. Chem. B* 103 (1999) 1270.
- [16] S.H. Garofalini, *J. Non-cryst. Solids* 120 (1990) 1.
- [17] B.P. Feuston, S.H. Garofalini, *J. Appl. Phys.* 68 (1990) 4830.
- [18] G.M. Rignanese, A. De Vita, J.C. Charlier, X. Gonze, R. Car, *Phys. Rev. B* 61 (2000) 13250.
- [19] Y.T. Xiao, A.C. Lasaga, *Geochim. Cosmochim. Acta* 60 (1996) 2283.
- [20] R. Koeny, *J. Phys. Chem. B* 105 (2001) 6221.
- [21] D.A. Litton, S.H. Garofalini, *J. Appl. Phys.* 89 (2001) 6013.
- [22] J.R. Rustad, E. Wasserman, A.R. Felmy, C. Wilke, *J. Coll. Interface Sci.* 198 (1998) 119.
- [23] J. Puibasset, J.-M. Pellenq, *J. Chem. Phys.* 118 (2003) 5613.
- [24] R. Jones, O. Gunnarsson, *Rev. Mod. Phys.* 61 (1989) 689.
- [25] M. Payne, M. Teter, D. Allan, T. Arias, J. Joannopoulos, *Rev. Mod. Phys.* 62 (1992) 1045.
- [26] M. Gillan, *Contemp. Phys.* 38 (1997) 115.
- [27] N.T. Barrett, C. Guillot, B. Villette, G. Treglia, B. Legrand, *Surf. Sci.* 251 (1991) 717.
- [28] J.E. Klepeis, L.J. Terminello, *Phys. Rev. B* 53 (1996) 16035.
- [29] L.N. Kantorovich, J.M. Holender, M.J. Gillan, *Surf. Sci.* 343 (1995) 221.
- [30] P.J.D. Lindan, J. Muscat, S. Bates, N.M. Harrison, M.J. Gillan, *Faraday Discuss.* 106 (1997) 135.
- [31] P.J.D. Lindan, N.M. Harrison, M.J. Gillan, *Phys. Rev. Lett.* 80 (1998) 762.
- [32] G. Kresse, J. Hafner, *Phys. Rev. B* 47 (1993) 5858.
- [33] G. Kresse, J. Hafner, *Phys. Rev. B* 49 (1994) 14251.
- [34] G. Kresse, J. Furthmüller, *Comput. Mater. Sci.* 6 (1996) 15.
- [35] G. Kresse, J. Furthmüller, *Phys. Rev. B* 54 (1996) 11169.
- [36] D. Vanderbilt, *Phys. Rev. B* 4 (1990) 7892.
- [37] G. Kresse, J. Hafner, *Condens. Matter* 6 (1994) 8245.
- [38] J.P. Perdew, J.A. Chevary, S.H. Vosko, K.A. Jackson, M.R. Pederson, D.J. Singh, C. Fiolhas, *Phys. Rev. B* 46 (1992) 6671.
- [39] N.H. de Leeuw, J.A. Purton, S.C. Parker, G.W. Watson, G. Kresse, *Surf. Sci.* 452 (2000) 9.
- [40] N.H. de Leeuw, J.A. Purton, *Phys. Rev. B* 63 (2001) 195417.
- [41] G.W. Watson, E.T. Kelsey, N.H. de Leeuw, D.J. Harris, S.C. Parker, *J. Chem. Soc. Faraday Trans.* 92 (1996) 433.
- [42] M. Born, K. Huang, *Dynamical Theory of Crystal Lattices*, Oxford University Press, Oxford, 1954.
- [43] B.G. Dick, A.W. Overhauser, *Phys. Rev.* 112 (1958) 90.
- [44] P.S. Baram, S.C. Parker, *Philos. Mag. B* 73 (1996) 49.

- [45] N.H. de Leeuw, S.C. Parker, *Phys. Rev. B* 58 (1998) 13901.
- [46] H. Ramberg, *J. Geol.* 62 (1954) 388.
- [47] D.R. Lide, *Handbook of Chemistry and Physics*, 81st ed., CRC Press, Boca Raton, USA, 2000.
- [48] W.A. Deer, R.A. Howie, J. Zussman, *An Introduction to the Rock-forming Minerals*, second ed., Longman, Harlow, UK, 1992.
- [49] M.V. Koudriachova, J.V.L. Beckers, S.W. de Leeuw, *Comput. Mater. Sci.* 20 (2001) 381.
- [50] W.C. Mackrodt, R.J. Davey, S.N. Black, R. Docherty, *J. Cryst. Growth* 80 (1987) 441.
- [51] P. Guenard, G. Renaud, A. Barbier, M. Gautier-Soyer, *Surf. Rev. Lett.* 5 (1998) 321.
- [52] N.H. de Leeuw, *Chem. Commun.* 17 (2001) 1646.
- [53] N.H. de Leeuw, G.W. Watson, S.C. Parker, *J. Chem. Soc. Faraday Trans.* 93 (1997) 467.
- [54] S.C. Parker, N.H. de Leeuw, S.E. Redfern, *Faraday Discuss.* 114 (1999) 381.
- [55] N.H. de Leeuw, S.C. Parker, *J. Am. Ceram. Soc.* 82 (1999) 3209.
- [56] B. Fubini, V. Bolis, M. Bailes, F. Stone, *Solid State Ion.* 32 (1989) 258.
- [57] J.A. Greathouse, R.J. O'Brien, G. Bemis, R.T. Pabalan, *J. Phys. Chem. B* 106 (2002) 1646.
- [58] N.H. de Leeuw, J.A. Purton, *Phys. Rev. B* 63 (2001) 5417.
- [59] T.G. Cooper, N.H. de Leeuw, *Surf. Sci.* 531 (2003) 159.
- [60] L.A. Curtiss, D.J. Frurip, M. Blander, *J. Chem. Phys.* 71 (1979) 2703.
- [61] C. Collins, W. Zhou, A.L. Mackay, J. Klinowski, *Chem. Phys. Lett.* 286 (1998) 88.
- [62] S. Thouvenel-Romans, O. Steinbock, *J. Am. Chem. Soc.* 125 (2003) 4338.